Applied Thermal Engineering 223 (2023) 119999

Contents lists available at ScienceDirect

Applied Thermal Engineering

journal homepage: www.elsevier.com/locate/apthermeng

Research Paper

Proposing and optimization of a parabolic trough solar collector integrated with a photovoltaic module layer

Gongxing Yan[a,b,c], Xia Zhou[b,c,*], Azher M. Abed[d,*], Theyab R Alsenani[e], Samia Elattar[f], Fan Peng[g,*], Mostafa A.H. Abdelmohimen[h,i]

[a] School of Intelligent Manufacture, Chongqing Creation Vocational College, Chongqing 402160, China
[b] School of Intelligent Construction, Luzhou Vocational and Technical College, Luzhou 646000, Sichuan, China
[c] Luzhou Key Laboratory of Intelligent Construction and Low-carbon Technology, Luzhou 646000, Sichuan, China
[d] Air Conditioning and Refrigeration Technologies Engineering Department, Al-Mustaqbal University College, Babylon 51001, Iraq
[e] Department of Electrical Engineering, College of Engineering in Al-Kharj, Prince Sattam Bin Abdulaziz University, Al-Kharj 11942, Saudi Arabia
[f] Department of Industrial & Systems Engineering, College of Engineering, Princess Nourah bint Abdulrahman University, P.O.Box 84428, Riyadh 11671, Saudi Arabia
[g] Sustainable Management of Natural Resources and Environment Research Group, Faculty of Environment and Labour Safety, Ton Duc Thang University, Ho Chi Minh City, Viet Nam
[h] Mechanical Engineering Department, College of Engineering, King Khalid University, Abha 61421, Saudi Arabia
[i] Shoubra Faculty of Engineering, Benha University, Cairo 11629, Egypt

A R T I C L E I N F O

Keywords:
Parabolic trough collector (PTC)
Photovoltaic (PV) module
Thermal
Electrical
Energy

A B S T R A C T

Parabolic trough collector (PTC) is a type of solar system that generates thermal energy by concentrating solar radiation on the surface of a circular receiver tube. However, the overall output of this solar system can be significantly enhanced by the integration of this system with Photovoltaic (PV) modules which is proposed and comprehensively investigated in this research using 3D validated numerical simulation. In the first step of this study, all operating parameters of the new PTC/PV system (i.e. thickness of the air gap, the glass cover thickness, copper nanoparticles mass fraction, and PV cell efficiency) are optimized by employing the Taguchi method. Afterward, it is attempted to enhance further the efficiency of the optimized PTC/PV system by rotating the receiver tube of the system and also installing metal foam inside the fluid channel of the receiver tube. According to the Taguchi method, the maximum overall performance of the PTC/PV system is 71.1%, when the glass cover thickness, air gap thickness, PV cell efficiency, and nanoparticles mass fraction are 2 mm, 10 mm, 21%, and 6%, respectively. Additionally, the numerical simulations show that rotating the receiver tube of the optimized PTC/PV system can augment the overall efficiency of the system from 71.1% to 82.5%, which is due to the improvement in heat transfer rate from the tube to the operating fluid. However, by rotating the receiver tube, the electrical efficiency of the PV cells reduces from 16.0% to 14.9%. Additionally, installing metal foam inside the receiver tube can boost the electrical and overall efficiency of the fixed PTC/PV system by approximately 2% and 13.9%, respectively. It is worth mentioning that adding foam to the rotating receiver tube declines the thermal efficiency of the system by around 0.5%.

1. Introduction

Solar energy has shown to be the greatest alternative energy sources to maintain the needed electrical energy. Solar energy is almost available everywhere and is free, clean, and environmentally friendly, all of which have made it an interesting and potential energy source in recent years.

In order for conversion of solar energy to electrical energy, different technologies are proposed by the engineers, such as flat plate collectors (FPC), parabolic trough collector (PTC), linear Fresnel reflectors (LFR), parabolic dish (PD), central receiver (CR), photovoltaic (PV) module, and photovoltaic thermal (PVT) system. Actually, each of these solar systems has its specific upside and downside potentials, which can be used for their particular climate condition and propose. PTC is a solar system used for medium and high-temperature applications. These systems are mostly used in solar power stations for steam generation to rotate the turbine for electrical generation purposes.

* Corresponding authors at: School of Intelligent Construction, Luzhou Vocational and Technical College, Luzhou 646000, Sichuan, China (X. Zhou).
E-mail addresses: 767509520@qq.com (X. Zhou), azhermuhson@uomus.edu.iq (A.M. Abed), SAElattar@pnu.edu.sa (S. Elattar), Pfanxu@gmail.com (F. Peng).

https://doi.org/10.1016/j.applthermaleng.2023.119999
Received 28 August 2022; Received in revised form 20 December 2022; Accepted 3 January 2023
Available online 6 January 2023
1359-4311/

Nomenclature

C_p	Specific heat capacity ($J \bullet kg^{-1} \bullet K^{-1}$)
D	Diameter of the fluid channel (m)
$\dot{E}$	Power (W)
F	Focal length (m)
G_k	Production of turbulence kinetic energy
k	Conductivity ($W \bullet m^{-1} \bullet K^{-1}$)
Nu	Nusselt number
P	Pressure of fluid (kPa)
S	Linear deformation of the liquid element
$\dot{S}_{gen}$	Entropy generation rate ($J \bullet m^{-1} \bullet s^{-1} \bullet K^{-1}$)
T	Temperature (K)
W	Aperture wide (m)
$\dot{W}_{el}$	Electrical power (W)
Greeks	
μ	Fluid dynamic viscosity ($Pa \bullet s$)
β	Volume fraction of liquid
$\varnothing$	Mass fraction of nanofluid
κ	Turbulent kinetic energy
$\in$	turbulent dissipation rate
η	Efficiency (%)
ρ	Material density ($kg \bullet m^{-3}$)
σ	Stefan-Boltzmann constant ($W \bullet m^{-2} \bullet K^{-4}$)
ε	Emissivity of material
φ	Rim angle (°)
Subscripts	
amb	Ambient
bf	Base fluid
el	Electrical
g	Glass cover
nf	nanofluid
r	Standard case
s	Solid
th	Thermal
w	Wind

Until now, some experimental studies are performed on the PTC to enhance their thermal performance via different methods. Chafie et al. [1], explored the thermal functionality of a parabolic trough collector under the Tunisian climate condition. The maximum thermal efficiency of the PTC was reported to be around 55%. Additionally, the average thermal efficiency on sunny and cloudy days was reported at 41% and 29%, respectively. In another study, Jamal-Abad et al. [2] studied the effect of embeding porous media in the parabolic trough collector's receiver on the Nusselt number and thermal funtionality of the PTC. They found that, by using metal foam in the PTC's receiver, the thermal efficiency of the system rises due to thermal conductivity increment. Based on their obtained data, although adding metal foam in the receiver tube raises the amount of Nusselt number, it increases the amount of friction factor significantly. The effect of using free porous, semi-porous, and full porous receivers in the PTC is investigated by Valizade et al. [3]. They reported that the temperature difference by using free porous, semi-porous, and full porous receivers is 3.3 °C, 8.8 °C, and 12.2 °C, respectively.

Besides, recently, some of the scholars assessed the influence of various parameters on the thermal performance of PTC using numerical methodology. The effect of employing supercritical CO_2 as a fluid for heat transfer to PTC is studied by Qiu et al. [4]. They observed that secondary flow occurs on the cross-section of the receiver tube due to buoyancy. Based on their study, the efficiency of the system is 81.93% up to 84.17% using the Rankine cycle. Bellos et al. [5] evaluated the performance of the PTC under the climate condition of Athens, Greece. They found that the maximum and minimum thermal efficiency belongs to June and December with 68.7% and 37.1%, respectively. In a separate investigation, Bellos and Tzivanidis [6] studied the performance of a PTC by using air and thermal oil as the working fluid. They conducted that the exergetic performance of the PTC with the working fluid of thermal oil and air is 31.57% and 25.62%, respectively. Also, the influence of using helical-screw tape inserts in a PTC system receiver is assessed by Raheem et al. [7]. In this work, the effect of various parameters of inserts, including helix angle, inner diameter, and insert thickness, on the functionality of the PTC system are evaluated. According to this study, the optimum value for the inserts accounted to be helix angle of 90°, inside diameter of 3.5 mm, and inserts thickness of 1 mm. Besides, the operation of the PTC system from the environmental and economic viewpoint is reviewed by Guillén-Lambea and Carvalho [8]. In this study, the Life Cycle Assessment (LCA) of the PTC system is scrutinized and the performance of the PTC system from the greenhouse gas emissions viewpoint is studied. In this research, they could propose a framework for the standards and provided the needed data for optimization of the PTC system with environmental considerations.

Based on the numerical and experimental studies, the nanoparticles dispersion in the base fluid increases the thermal properties of the working fluid, which increases the thermal and electrical efficiencies of the solar systems [9]. Allouhi et al. [10] investigated the influence of using various nanofluids in the PTC's receiver on its thermal performance. They found that the dispersion of nanofluid in the fluid base with a concentration of 3% has only a minor effect on the system's thermal efficiency. Moreover, they observed that the system's exergy efficiency with pure base fluid is between 3.0% and 8.5%, while the exergy efficiency of the system using CuO nanoparticles is approximately 9.0%. Moreover, the performance of a nanofluid-based PTC system with a rotary absorber tube is investigated by Bezaatpour et al. [11]. In this work, in order to augment the functionality of the PTC system, an external magnetic field is imposed on the absorber tube of the system. Based on the results, it is concluded that in the low rotational speeds of the absorber tube, by increasing the intensity of the magnetic field from 0 to 1000 G, the exergy destruction of the system reduces remarkably. While, in high rotational speeds, the variation of magnetic field intensity do not significantly influence the PTC system performance. Also, it is found that the PTC system heat loss with rotary absorber under the effect of a magnetic field is about 37% lower than that of a PTC system with fixed absorber tube without no magnetic field.

Although PTCs can maintain the needed steam of the turbine in the power stations for electrical generation, some solar systems, such as PV modules, can directly convert solar energy into electrical energy. However, the PV modules depend on their working temperature in terms of electrical efficiency [12]. In fact, by raising the PV cell temperature, the amount of PV module electrical efficiency is reduced. Thus, some researchers tried to elevate the electrical efficiency of these systems by combining them with solar collectors (PVT systems) by lowering their cell temperature. In Table 1, there are some experimental and numerical studies on the performance of this type of solar system.

Based on the studies mentioned above, by the combination of PTC and PV module, not only the PV cells temperature will reduce, but also it is possible to produce electrical energy directly (PV) and indirectly (steam production) simultaneously with a single device. Recently, some limited mathematical studies are performed on this type of solar system. Soltani et al. [17] studied the effect of using the PV module layer and thermoelectric generator in the PTC's receiver. Based on their

Table 1
A summary of works on PVT systems.

Ref.	Methodology	Novelty	Concluding remarks
Sarafraz et al. [13] (2019)	Exp.	Using MWCNT/water in the PVT system	The electrical and thermal energy production of the MWCNT/water-based PVT system is reported to be 17% and 120% higher than the water-ethylene glycol-based PVT system.
Al-Waeli et al. [14] (2019)	Exp.	Using SiC/water in the PVT system	The highest obtained electrical and thermal efficiencies were reported to be 13.7% and 72%, respectively.
Salari and Hakkaki-Fard [15] (2019)	Num.	Investigation of the effect of different parameters on the performance of the PVT system.	Heat transfer mass flow rate, solar radiation, and ambient temperature were announced to be the favorable parameters of thermal efficiency. Besides, wind speed and heat transfer mass flow rate were reported to be favorable parameters.
Salari et al. [16] (2020)	Num.	Using of the thermoelectric generator in the PVT system	The electrical efficiency of the PVT and PVT/TE are 13.58 and 14.71%, respectively, at a particular working condition. However, the thermal efficiency of the PVT and PVT/TE are 55.28% and 53.26%.
Soltani et al. [17] (2018)	Num.	Using the TE generator and PV module in the PTC's circular receiver	The solar radiation on the receiver is assumed to be uniform. Using a 1D numerical method.
Valizadeh et al. [18] (2019)	Num.	Using a PV module in a triangular receiver of a PTC	The commercial PTC receivers are generally circular. Using a 1D numerical method.

Table 2
Thermophysical properties of the components of the system [19,20]

System component	Density ($kg \bullet m^{-3}$)	Conductivity ($W \bullet m^{-1} \bullet K^{-1}$)	Specific heat ($J \bullet kg^{-1} \bullet K^{-1}$)
Glass cover	2200	0.76	830
PV layer	2330	148	700
Air gap	1.225	0.024	1006.43
Absorber and copper foam	8960	401	385

investigation, the maximum amount of thermal and electrical power are about 240 W and 20.5 W, respectively. In another study, Valizadeh et al. [18] studied the effect of using a PV module layer in a triangular receiver tube of a PTC. They found that the maximum amount of exergy efficiency is about 30.3%. Additionally, they found that by increasing the fluid velocity, the electrical and thermal efficiency of the system rises 1.05% and 2.2%, respectively. Table 2 reveals the novelty and disadvantages of the performed studies on the combined PTC.

Based on the foregoing literature review, extensive investigations have been performed on evaluating the thermal performance of the commercial PTC system. However, the overall performance of the typical PTC system is not high enough, and enhancement in the output of this system can significantly expand the installation of it around the globe. Therefore, the primary purpose of the present research is to present a type of PTC system that can simultaneously provide thermal and electrical power. This way, a PTC system is integrated with a PV module. Additionally, to present a PTC/PV system with the most optimized electrical and thermal output, the dimensions of the various specifications of the system, including glass thickness and air thickness, are optimized using the Taguchi method.

For the first time in the present study, not only the specifications of the PTC/PV system are optimized, but also the effect of using metal foam on the operation of the system is scrutinized. In fact, using metal foam inside the fluid channel can boost the heat transfer from the receiver tube to the working fluid, providing higher thermal and electrical output by the hybrid system. Furthermore, for higher enhancement of the functionality of the PTC/PV system, the influence of rotating the receiver tube on the outputs of the system is evaluated. The key novelties of this study are listed as:

- Combining a parabolic trough collector with a PV module.
- Optimization of the PTC/PV system by employing the Taguchi method.
- Evaluation of the electrical, thermal, and overall performance of the optimized PTC/PV, OPTC/PV system with rotational absorber, and OPTC/PV system with both rotational absorber and copper foam.
- Investigation of the influence of Cu/water nanofluid on the performance of the PTC/PV.
- Investigation of Nu number and entropy generation over the absorber channel of the systems.

2. Numerical simulation

In present section, the specifications of the designed PTC/PV system, governing equations, solar radiation distribution over the surface of the circular receiver, and the imposed boundary conditions on the numerical models are discussed.

2.1. Receiver tube

In order to investigate the functionality of the PTC/PV system, its receiver tube is three-dimensionally designed as shown in Fig. 1. Based on this figure, the designed receiver tube consists of a glass cover layer, an air gap, a PV layer, an absorber, and a fluid channel. In order to comprehensively investigate the functionality of the PTC/PV system, in the first step, the specifications of the PTC/PV system are optimized using the Taguchi method. For the optimization of the system, the considered parameters are the thickness of the air gap, the thickness of the glass cover, the nanoparticles mass fraction, and the efficiency of the PV module. Henceforth, the effect of using a rotational absorber on the performance of the optimized PTC/PV system (OPTC/PV system) is evaluated. Besides, in another case, the effect of installing copper metal foam on the functionality of the OPTC/PV system with a rotational tube is revealed. Thermophysical properties and dimensions of the components of the PTC/PV system are available in Tables 2 and 3, respectively. It should be noted that the porosity and permeability of the copper foam are considered 0.9 and 7×10^{-6}, respectively.

For the numerical simulations, the base fluid of the system is considered to be Therminol VP-1, which its properties in the range of $285.15 \text{ K} \leq T \leq 698.15 \text{ K}$ are as follows [21]:

Heat capacity ($J \bullet kg^{-1} \bullet K^{-1}$):

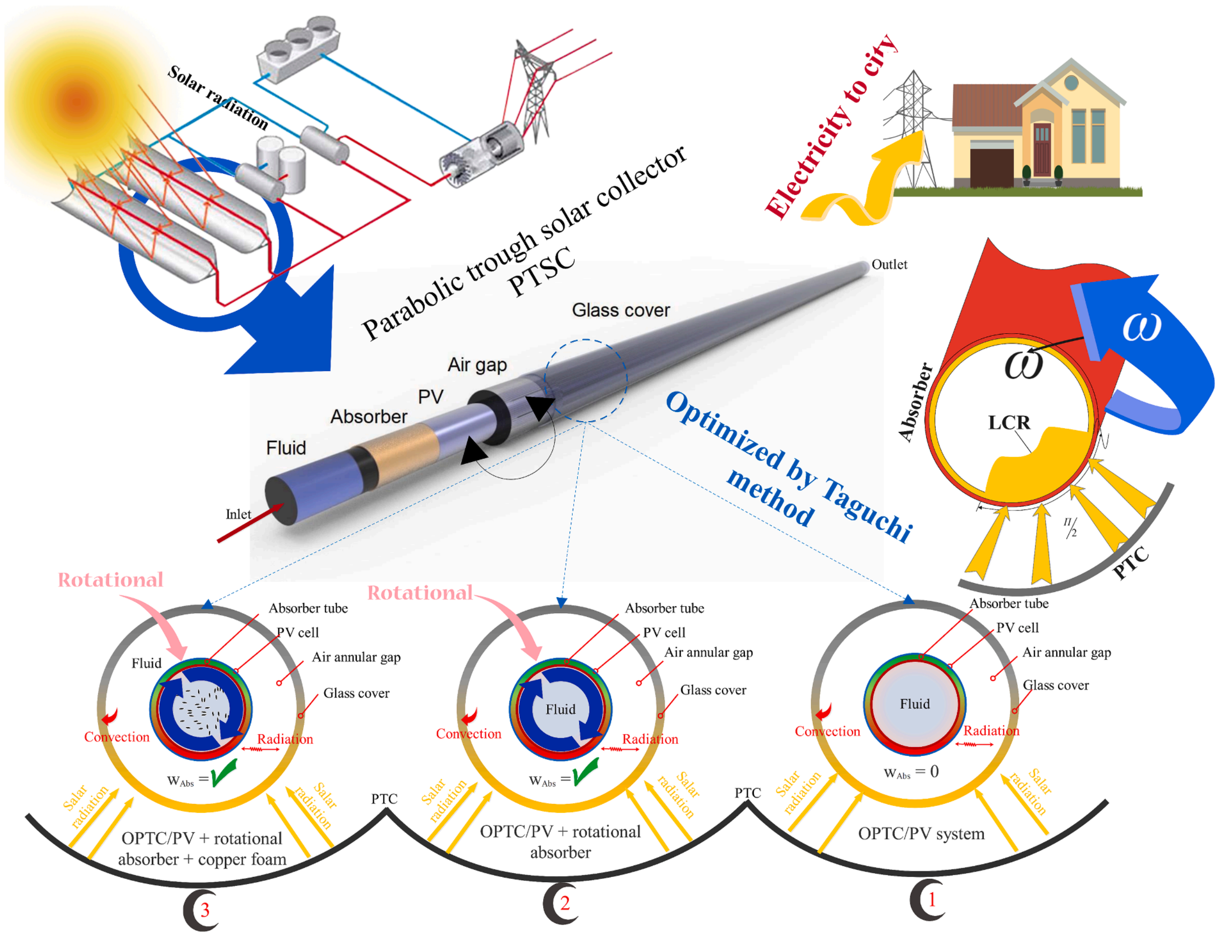

Fig. 1. PTC/PV receiver tube, (1) optimized PTC/PV system by using Taguchi method, (2) OPTC/PV system with rotational absorber, and (3) OPTC/PV system with both rotational absorber and copper foam.

Table 3
Dimensions of the different components of the PTC/PV system.

System component	Dimension (mm)
Diameter of channel	80
Thickness of Absorber	2
Thickness of the PV module	0.3
Thickness of air gap	5–40
Thickness of Glass cover	2–6
Length of the receiver tube	5,000

$$C_p = 2.125\times10^3 - 11.017T + 0.049862T^2 - 7.7663\times10^{-5}T^3 + 4.394\times10^{-8}T^4 \quad (1)$$

Density ($kg \bullet m^{-3}$):

$$\rho = 1.4386\times10^3 - 1.8711T + 2.273\times10^{-3}T^2 - 2.3793\times10^{-6}T^3$$

Thermal conductivity ($W \bullet m^{-1} \bullet K^{-1}$):

$$\lambda = 0.14644 + 2.0353\times10^{-5}T - 1.9367\times10^{-7}T^2 + 1.0614\times10^{-11}T^3 \quad (3)$$

The viscosity of the Therminol VP-1 in the range of 285.15 K $\leq T \leq$ 373.15 K is [21]:

$$\text{Viscosity } (mPa \bullet s) \quad \mu = 3.661\times10^2 - 3.0154T + 8.3409\times10^{-3}T^2 - 7.723\times10^{-6}T^3$$

Also, in the range of 373.15 K $\leq T \leq$ 698.15, the viscosity of the fluid can be obtained as [21]:

$$\text{Viscosity } (mPa \bullet s) \quad \mu = 23.165 - 0.1476T + 3.617\times10^{-4}T^2 - 3.9844\times10^{-7}T^3 + 1.6543\times10^{-10}T^4 \quad (5)$$

Moreover, the nanoparticle dispersion in the base fluid increases the thermal properties of the operating fluid, which causes enhancement of the overall performance of the solar system [22,23]. Thus, to augment the performance of the PTC/PV system, Cu nanoparticles with mass fractions in the range of 0–6% are dispersed in the base fluid. The heat capacity, density, thermal conductivity, and viscosity of the nanofluid can be calculated as Eq. (6–9) in which ϕ is the mass fraction of the nanoparticle, d_p and d_{bf} are nanoparticle and base fluid diameters, respectively, and, k_B represents the Boltzmann constant (1.381 $\times$ 10^{-23} J/K).

Heat capacity [24]:

$$C_{p,nf} = (1-\phi)C_{p,bf} + \phi C_{p,nf} \quad (6)$$

Density [24]:

$$\rho_{nf} = (1-\phi)\rho_{bf} + \phi\rho_{nf} \quad (7)$$

Thermal conductivity [25]:

$$k_{nf} = \left[\frac{k_p + 2k_{bf} - 2\phi(k_{bf} - k_p)}{k_p + 2k_{bf} + \phi(k_{bf} - k_p)} + \frac{\rho_p \phi C_{p,bf}}{2k_{bf}}\sqrt{\frac{2k_B T}{3\pi d_p \mu_{bf}}}\right]k_{bf} \quad (8)$$

Viscosity [26]:

Table 4
Thermal properties of the Cu nanoparticles.

Property	Value
Density ($kg \bullet m^{-3}$)	10,500
Thermal conductivity ($W \bullet m^{-1} \bullet K^{-1}$)	429
Heat capacity ($J \bullet kg^{-1} \bullet K^{-1}$)	235

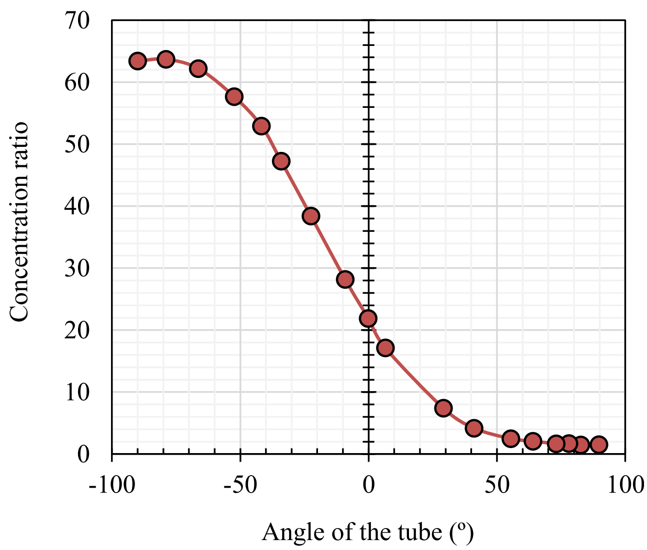

Fig. 2. Solar radiation distribution over the PV module.

$$\mu_{nf} = \frac{\mu_{bf}}{1 - 34.87\left(\frac{d_p}{d_{bf}}\right)^{-0.3}\phi^{1.03}}\mu_{bf} \tag{9}$$

The Cu nanoparticle thermal properties are presented in Table 4.

2.2. Parabolic reflector

In order to apply the effect of parabolic reflector geometry, such as aperture wide and rim angle, on the distribution of the solar radiation over the receiver tube, the Soltrace software is used. By using this software, the solar radiation distribution as a function of a circular angle is obtained. In this open-source software, 4×10^6 solar rays are generated and tracked to obtain the distribution of solar rays over the tube accurately. For this simulation, inserting the value of the optical properties of different components of the receiver tube is necessary. For this purpose, the transmissivity and emissivity of the glass cover is considered 0.97 and 0.86 [21], respectively, and the absorptivity of the PV layer and absorber is taken 0.95 [27]. The amount of distribution of the solar radiation over the PV module layer of the system is presented in Fig. 2.

Additionally, the profile of the reflector of the PTC/PV system is considered to be a parabola in which its focal length can be calculated as [28]:

$$x^2 = 4Fy \tag{10}$$

$$F = \frac{W}{4tan(\varphi/2)} \tag{11}$$

In these equations, F, W, and φ represent the focal length, aperture wide, and rim angle, respectively. Also, the concentration ratio of the system solar radiation can be obtained as [28]:

$$C = \frac{W}{d_{pv}} \tag{12}$$

where, d_{pv} is the diameter of the PV layer. In this study, the concentration of the system is considered to be 100.

2.3. Governing equations

To simulate the receiver tube with the highest accuracy, the tube is designed three-dimensionally and simulated with a steady-state model. For the liquid zone, due to the heat transfer fluid high Reynolds number in the fluid channel, the $\kappa - \varepsilon$ turbulence model is used for the solution of the governing equations. In the following, the continuity, momentum, and energy equations for the fluid zone are presented [29]:

$$\frac{\partial(\rho\bar{u}_i)}{\partial x_i} = 0 \tag{13}$$

$$\frac{\partial(\rho\bar{u}_i\bar{u}_j)}{\partial x_j} = -\frac{\partial\bar{P}}{\partial x_i} + \frac{\partial}{\partial x_j}\left[\mu\left(\frac{\partial\bar{u}_i}{\partial x_j} + \frac{\partial\bar{u}_j}{\partial x_i}\right) - \frac{2}{3}\mu\frac{\partial\bar{u}_i}{\partial x_i}\delta_{ij} - \rho\overline{u_i^{'}u_j^{'}}\right] \tag{14}$$

$$\frac{\partial(\rho\bar{u}_jc\bar{T})}{\partial x_j} = \frac{\partial}{\partial x_j}\left(\lambda\frac{\partial\bar{T}}{\partial x_j} + \frac{\mu_t}{\sigma_{h,t}}\frac{\partial(c\bar{T})}{\partial x_i}\right) - \bar{u}_j\frac{\partial\bar{P}}{\partial x_j} + \left[\mu\left(\frac{\partial\bar{u}_i}{\partial x_j} + \frac{\partial\bar{u}_j}{\partial x_i}\right) - \frac{2}{3}\mu\frac{\partial\bar{u}_i}{\partial x_i}\delta_{ij} - \rho\overline{u_i^{'}u_j^{'}}\right]\frac{\partial\bar{u}_i}{\partial x_i} \tag{15}$$

The amount of turbulent kinetic energy (κ) and turbulent dissipation rate (ϵ) can be calculated as [29,30]:

$$\frac{\partial(\rho k\bar{u}_j)}{\partial x_j} = \frac{\partial}{\partial x_j}\left[\left(\mu + \frac{\mu_t}{\sigma_k}\right)\frac{\partial k}{\partial x_j}\right] + G_k - \rho\epsilon \tag{16}$$

$$\frac{\partial(\rho\varepsilon\bar{u}_j)}{\partial x_j} = \frac{\partial}{\partial x_j}\left[\left(\mu + \frac{\mu_t}{\sigma_\epsilon}\right)\frac{\partial\epsilon}{\partial x_j}\right] + \rho C_1 S\epsilon - \rho C_2\frac{\epsilon^2}{k + \sqrt{\nu\epsilon}} \tag{17}$$

where,

$$C_1 = max\left[0.43, \frac{\eta}{\eta + 5}\right] \tag{18}$$

$$\eta = S\frac{k}{\varepsilon} \tag{19}$$

$$S \equiv \sqrt{2S_{ij}S_{ji}} \tag{20}$$

$$G_k = -\rho\overline{u_i^{'}u_j^{'}}\frac{\partial\bar{u}_j}{\partial x_i} \tag{21}$$

In the above equations, G_k represents the production of turbulence kinetic energy, S_{ij} donates the linear deformation rate of a fluid element. Besides, in these equations, $C_2 = 1.9$, $\sigma_k = 1$, and $\sigma_\varepsilon = 1.2$ [21]. Moreover, the governing equation for the solid layers of the system can be presented as [31]:

$$\nabla \bullet (k\nabla T) + \psi\dot{E}_{sun} - \xi\dot{E}_{el} = 0 \tag{22}$$

here, $\dot{E}_{sun}$ is input solar energy to the system and $\dot{E}_{el}$ is electrical production by the PV cells. In this equation, the amount of ψ and ξ is equal to 1 for the PV layer and 0 for the other layers [31], due to the presence of heat absorption and electrical generation only in this system component.

2.4. Boundary condition

For modeling the systems in the software, imposing proper boundary conditions is required. In this geometry, the inlet of the fluid channel is considered to be the "mass flow inlet," and at the channel outlet, the "outlet pressure" condition is applied. The amount of electrical energy production in the PV layer is also extracted from thesystem energy balance by using a UDF code. It is noteworthy that the amount of calculation of the electrical energy production of the system is explained in the following section.

Besides, for the glass cover surface, the "wall" boundary condition with the "mixed heat transfer mechanism" is used. In this kind of

Table 5
Boundary conditions employed in the simulation.

Parts	Condition
Glass cover	Wall with mixed heat transfer
Inlet	Mass flow inlet
outlet	Pressure outlet
PV cells	Heat generation
Contacts of the surfaces	Interface

Table 6
Base case conditions.

Parameter	Vale
Solar radiation	$1000\ W \bullet m^{-2}$
Mass flow rate	$0.3\ kg \bullet s^{-1}$
Inlet temperature	30 °C
Concentration ratio	100
Wind speed	$1\ m \bullet s^{-1}$
Rotational speed	$0.5\ rad \bullet s^{-1}$

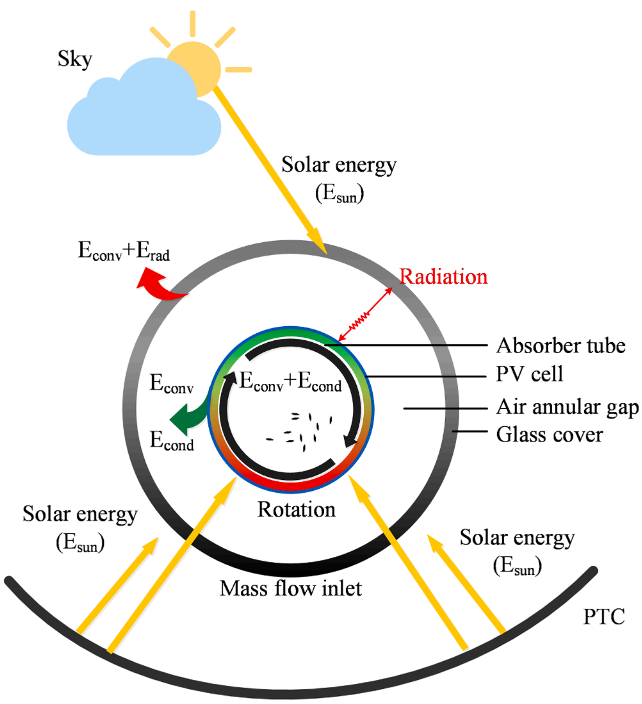

Fig. 3. Heat transfer mechanisms in the PTC/PV system.

boundary condition, the glass cover will be able to lose its heat to the surronding through both mechanisms of radiation and convection. The imposed boundary conditions on the systems are summarized in Table 5.

To obtain the amount of convection heat transfer coefficient on the glass cover surface, the equation of Mullick and Nanda is used [32]. Based on this equation, the coefficient of convection heat transferover a circular tube depends on the wind speed and the diameter of the tube [32]:

$$h_w = V_w^{0.58} d_g^{-0.42} \tag{23}$$

Additionally, to calculate the amount of the tube heat loss to the surronding by radiation mechanism, the amount of sky temperature should be determined. The sky temperature is dependent on the ambient temperature and can be expressed as [33]:

$$T_{sky} = 0.0522 T_{amb}^{1.5} \tag{24}$$

By calculating the sky temperature, the amount of heat transfer to the environment is determined by using Stefan Boltzmann's law. It is noteworthy to mention that in the parametric analysis of the systems, only one parameter is variable, and all other operating factors of the systems are as same as the base case conditions, which are provided in Table 6.

2.5. Thermodynamic analysis

The thermodynamic analysis of the PTC/PV system based on the first law of thermodynamics is discussed in this section. By assuming the system to be a control volume, the balance of energy for the system can be presented as [9]:

$$\dot{E}_{sun} = \dot{E}_{el} + \dot{E}_{th} + \dot{E}_{loss} \tag{25}$$

here, $\dot{E}_{th}$, and $\dot{E}_{loss}$ are the output thermal energy and the system heat loss, respectively. The thermal output of the system can be obtained as [15]:

$$\dot{E}_{th} = \dot{m}\left(h_{mass,out} - h_{mass,in}\right) \tag{26}$$

In this equation, $h_{mass,in}$ and $h_{mass,out}$ refer to the enthalpy of working fluid and the inlet and outlet of the receiver tube, respectively, and $\dot{m}$ donates the fluid mass flow rate in the channel. Furthermore, the input solar energy amount can be determined as:

$$\dot{E}_{sun} = 2\int_{-90}^{90} \dot{G}_{sun,con}(\theta) d\theta \bullet \alpha_{cell} \bullet \tau_{glass} \tag{27}$$

As mentioned above, the amount of input solar radiation is dependent on the integral of the concentrated solar radiation over the receiver tube surface, the absorption coefficient of the PV cell (α_{cell}) and the the glass cover transmissivity (τ_{glass}). Also, the thermal loss of the PTC/PV system can be calculated as [34]:

$$\dot{E}_{loss} = \dot{E}_{conv,glass} + \dot{E}_{rad,glass} \tag{28}$$

$$\dot{E}_{conv,glass} = h_w \bullet A \bullet \left(T_{glass} - T_{sky}\right) \tag{29}$$

$$\dot{E}_{rad,glass} = \sigma \bullet \varepsilon \bullet A \bullet \left({T_{glass}}^4 - {T_{sky}}^4\right) \tag{30}$$

where, $\dot{E}_{conv,glass}$ and $\dot{E}_{rad,glass}$ refer to the heat loss of the PTC/PV system through convection and radiation, respectively. In these equations, σ is the constant of Stefan-Boltzmann, ε is the glass cover emissivity, and T_{glass} donates temperature of the glass envelope. The heat transfer mechanisms in the PTC/PV system are illustrated in Fig. 3.

According to the presented equations, the amount of thermal efficiency of the PTC/PV system can be presented as:

$$\eta_{th} = \frac{\dot{E}_{th}}{\dot{E}_{sun}} = \frac{\dot{m}\bullet\left(h_{mass,out} - h_{mass,in}\right)}{2\int_{-90}^{90} \dot{G}_{sun,con}(\theta) d\theta \bullet \alpha_{cell} \bullet \tau_{glass}} \tag{31}$$

Besides, the PV module electrical efficiency is highly dependent on its temperature [35]. In fact, an increment in the PV cell temperature, reduces its electrical efficiency [36]. An empirical equation is used to obtain the PV module's electrical efficiency. In this equation, the PV module electrical efficiency based on its temperature (T_{cell}) and standard electrical efficiency (η_r), which written in the following [37]:

$$\eta_{el} = \frac{\dot{W}_{el}}{\dot{E}_{sun}} = \eta_r \bullet \left[1 - 0.0045 \bullet \left(T_{cell} - 298.15\right)\right] \tag{32}$$

In this equation, the standard electrical efficiency of the silicon PV module is taken to be 15% [36]. Finally, the overall efficiency of the PTC/PV system can be calculated as follows:

$$\eta_{ov} = \eta_{el} + \eta_{th} \tag{33}$$

Furthermore, the amount of entropy generation over the absorber tube can be obtained by [38]:

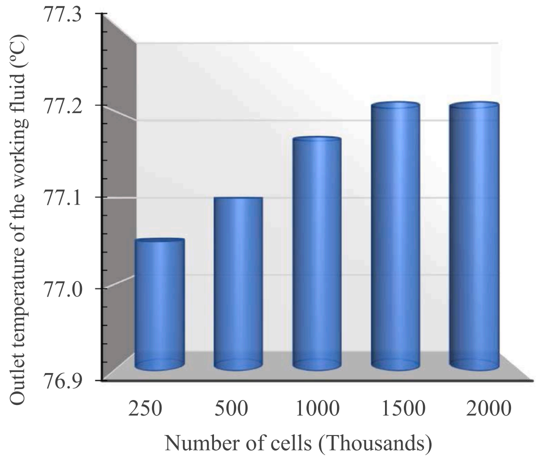

Fig. 4. The outlet temperature of the working fluid versus the number of cells.

Table 7
Specifications of the SEGS LS-2 PTCs [43].

System component	Dimension (mm)
Size of reflector	7.8 × 5
Focal length	1.84
Radios of the glass cover	0.0575
Radios of absorber	0.0350
Thickness of absorber	0.002

Table 8
The details of the optimization method.

Parameter	Level 1	Level 2	Level 3	Level 4
Thickness of the glass cover (mm)	2	3	4	6
Thickness of the air gap (mm)	5	10	20	40
PV cell efficiency (%)	15	17	19	21
Mass fraction of the Cu/Water nanofluid (%)	0	2	4	6

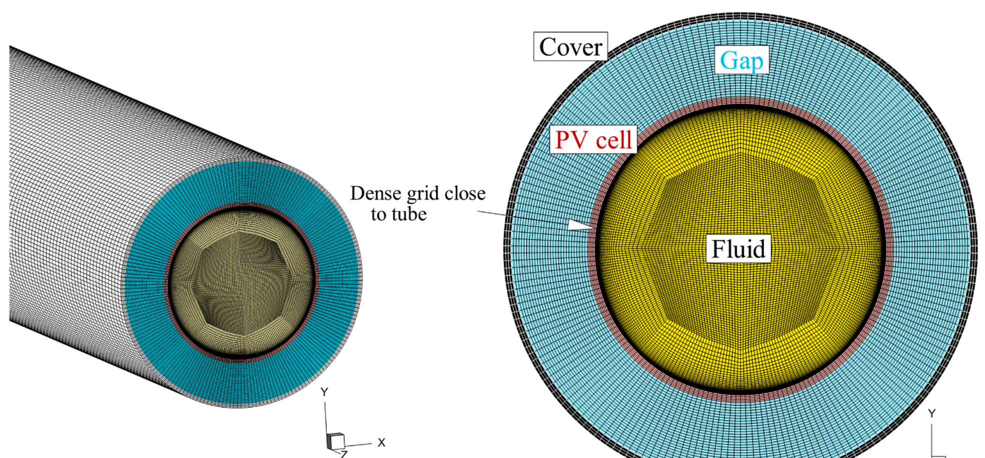

Fig. 5. The mesh distribution over the PTC/PV system.

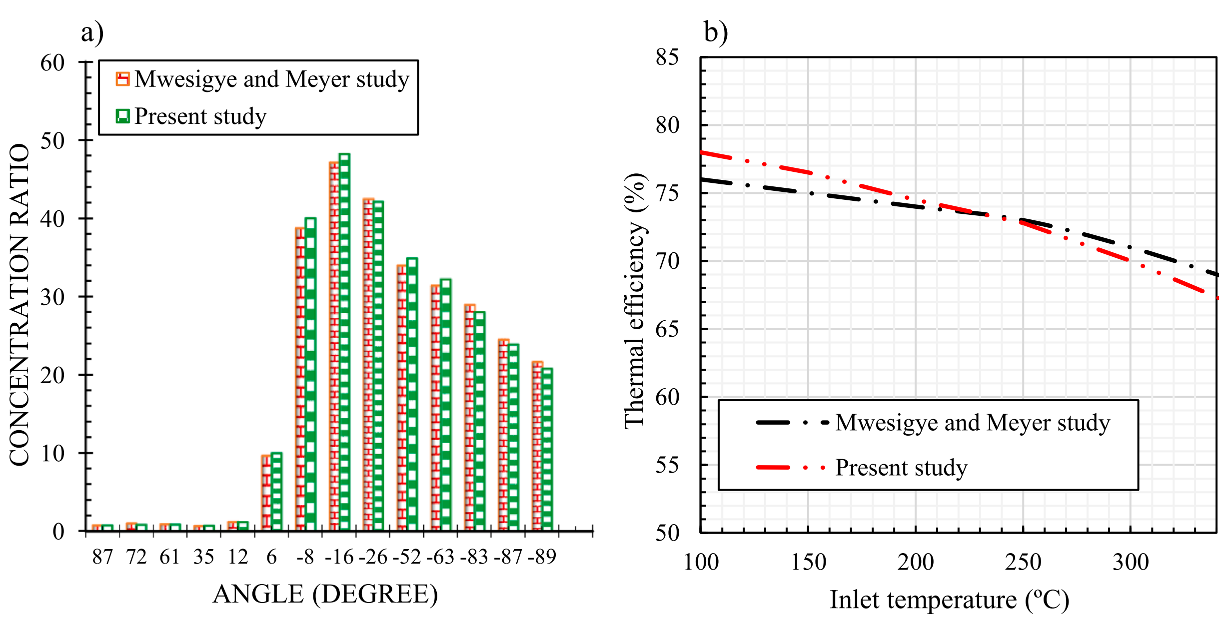

Fig. 6. (a) Solar radiation distribution over the surface of the absorber of the PTC/PV system in the present study and Mwesigye and Meyer [21], (b) thermal efficiency of the PTC system versus inlet temperature in the present study and Mwesigye and Meyer [21]

Table 9
The orthogonal array for the optimization of the PTC/PV system by the Taguchi method.

Test	A	B	C	D	Thermal efficiency (%)	Electrical efficiency (%)	Overall efficiency (%)	$T_{Bulk}(K)$	$h(W/m^2K)$	Nu	$S^{'}_{gen}(W/mK)$
1	1	1	1	1	57.23	10.18	67.40	326.76	492.36	302.99	33.73
2	1	2	2	2	56.43	12.35	68.77	326.84	656.61	293.46	34.81
3	1	3	3	3	55.65	14.43	70.08	326.93	855.87	298.99	34.15
4	1	4	4	4	54.36	16.38	70.74	326.81	1044.27	296.25	34.49
5	2	1	2	3	55.46	12.57	68.03	326.85	724.06	252.95	40.38
6	2	2	1	4	57.04	11.35	68.38	327.97	869.44	246.65	41.13
7	2	3	4	1	55.02	14.87	69.90	325.85	568.47	349.83	29.38
8	2	4	3	2	54.90	14.21	69.11	326.20	753.39	336.71	30.46
9	3	1	3	4	55.91	14.22	70.13	327.48	793.61	225.14	45.19
10	3	2	4	3	55.14	15.81	70.96	326.71	802.05	280.19	36.49
11	3	3	1	2	56.77	11.02	67.79	326.99	702.15	313.81	32.52
12	3	4	2	1	55.83	12.06	67.90	326.18	577.72	355.52	28.85
13	4	1	4	2	55.45	15.14	70.59	326.43	625.30	279.46	36.64
14	4	2	3	1	55.77	13.25	69.03	326.16	538.31	331.27	30.96
15	4	3	2	4	56.25	13.03	69.29	327.63	944.10	267.83	37.96
16	4	4	1	3	56.48	11.41	67.89	327.28	876.30	306.13	33.28

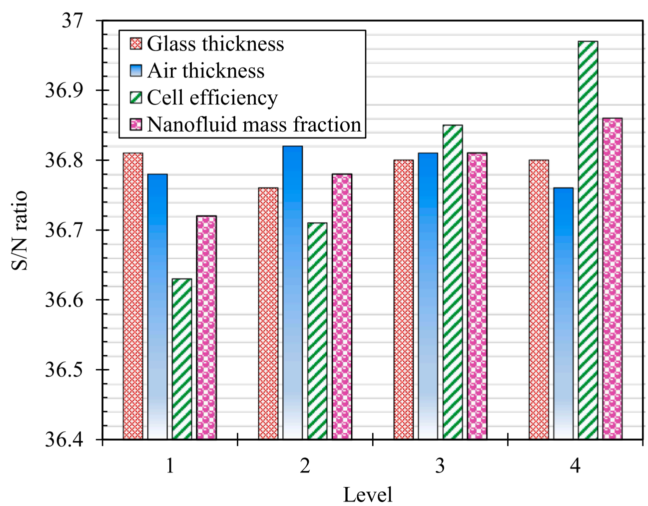

Fig. 7. The amount of signal to noise (S/N) ratios for the studied parameters.

$$\dot{S}_{gen} = \frac{\dot{q}}{\pi\lambda {T_{balk}}^2 Nu} + \frac{32\dot{m}^3 c_f}{\pi^2\rho^2 T_{bulk} D^5} \tag{34}$$

where [34],

$$Nu = \frac{hD}{k} \tag{35}$$

$$h = \frac{\ddot{q}}{T_w - T_{bulk}} \tag{36}$$

$$T_{bulk} = \frac{T_{in} - T_{out}}{2} \tag{37}$$

$$c_f = \frac{(-dp/dx)}{\rho D/2G^2} \tag{38}$$

$$G = \frac{4\dot{m}}{\pi D^2} \tag{39}$$

In the above equations, D and $\dot{q}$ represents the diameter of the fluid channel and heat transfer rate per length, respectively.

3. Taguchi method

Taguchi method is one of the practical models that can be used for the optimization of engineering systems. This method makes it possible to determine the best operating conditions of a system with a limited number of tests or simulations. Using the Taguchi method not only reduces the effects of uncontrollable factors but also decreases the amount of time and money costs [39,40]. In this method, the number of factors and their level should be determined at the first step. In this study, the considered parameters are (A) thickness of the glass cover, (B) thickness of the air gap, (C) PV cell efficiency, and (D) mass fraction of the Cu nanoparticles. Next, the list of required tests is obtained from the software (Minitab 19). Afterward, by performing the proposed simulations, the overall system efficiency (objectives parameter) should enter again into the software. Finally, the amount of effect of variation of each parameter on the output results (overall efficiency) and the best operating condition of the system will be determined.

In this method, the number of needed minimum simulations (*NE*) is dependent on various parameters, including the number of parameters (*NP*) and the number of levels of each parameter (*NL*), which can be obtained as following [41]:

$$NE = 1 + NP(NL - 1) \tag{40}$$

Also, the amount of S/N ratio that determines the amount of effect of each parameter on the output results can be obtained using Eq. (37) [42] in which n donates the number of repetition and y_i is the result of each test.

$$\frac{S}{N} = -10log\left(\frac{1}{n}\sum_{i=1}^{n}\frac{1}{y_i^2}\right) \tag{41}$$

4. Mesh independency and validation

This section discusses the independence of the output numerical results from the number of cells and the validity of the results. In order to achieve mesh independency, the geometry of the PTC/PV system was meshed with 250, 500, 1000, 1500, and 2000 thousand cells and simulated under the solar radiation concentration ratio of 100 and inlet flow temperature of 30 °C. Also, the thickness of the glass cover and air gap is considered to be 2 mm and 5 mm, respectively. Fig. 4 presents the amount of operating fluid outlet temperature versus the number of cells.

As depicted in Fig. 4, by increasing the cell number, the operating fluid outlet temperature rises. Due to the high-temperature gradient in the air gap and fluid change, larger cells cannot accurately predict the temperature distribution over the system.Thus, a dense mesh for the PTC/PV system is necessary. According to the output results, the number of 1500 thousand cells for the meshing of the PCT/PV system is suitable. It should be noted that for the meshing of other PTC/PV systems with different component sizes, the same mesh density (not cell number) is applied.

The distribution of mesh over the PTC/PV system is depicted in Fig. 5. As demonstrated in this figure, the system has meshed with

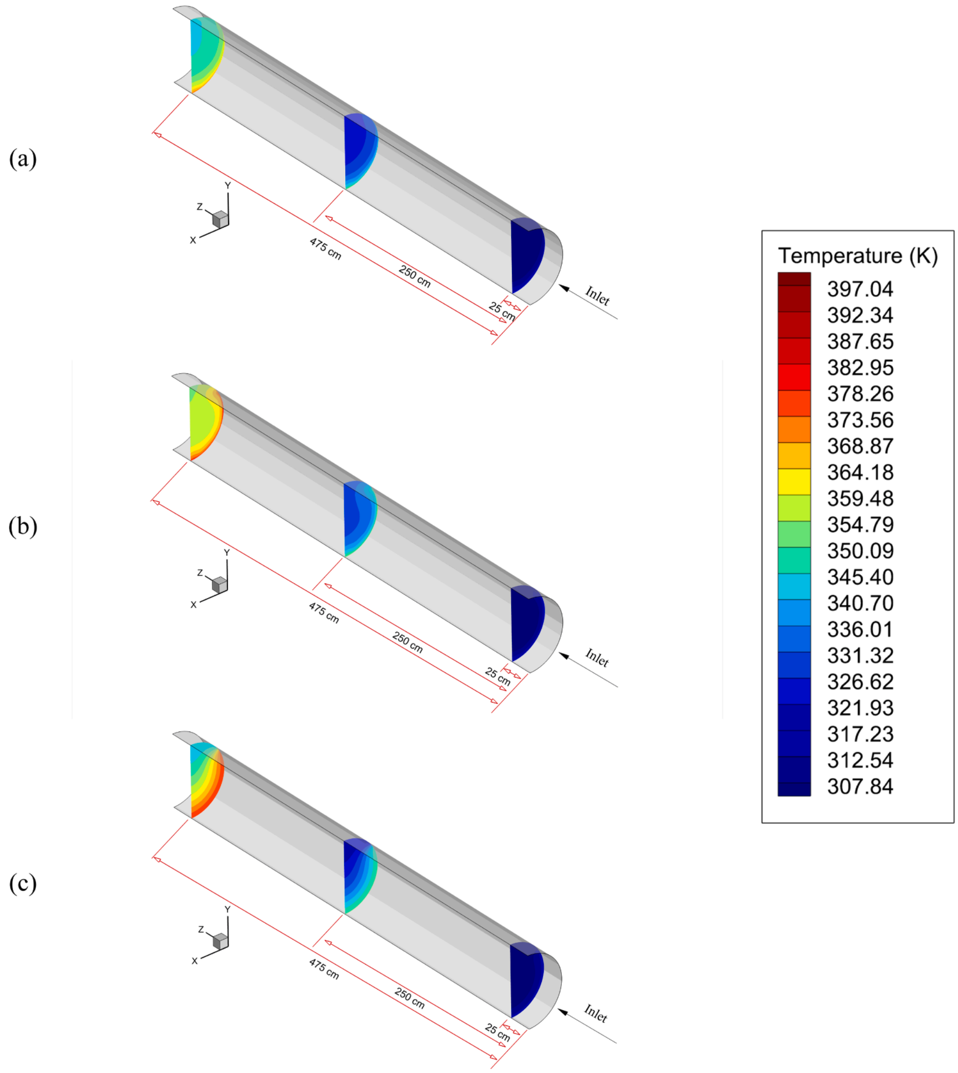

Fig. 8. The temperature distribution of the fluid channel at the different cross-sections in the (a) OPTC/PV system, (b) OPTC/PV system with rotational absorber, and (c) OPTC/PV system with both rotational absorber and copper foam.

hexahedron cells, and some thin layers of cells are generated in the fluid channel near the wall of the PV module. These thin layers are generated due to the high velocity and temperature gradient in this area.

Besides, to present reliable results, comparing the outputs of the current work with the results of the other research should be carried out. For the validation of the results, the properties, size of the components, and working conditions of the system are assumed to be as same as the reference study. In Fig. 6(a), the amount of solar radiation concentration over the surface of the PTC/PV system in the present study and the study of Mwesigye and Meyer [21] is depicted. According to this figure, the minimum, maximum, and average error between the two studies is approximately 0.8%, 4.03%, and 2.43%, respectively.

Furthermore, the amount of thermal efficiency of the simulated PTC (SEGS LS-2) in terms of the operating fluid inlet temperature for the current work and the study of Mwesigye and Meyer [21] is presented in Fig. 6(b). Based on the numerical simulations, the minimum, maximum, and average error between the present study and the study of Mwesigye and Meyer [21] is approximately 0.27%, 2.94%, and 1.65%, respectively. The specifications of the SEGS LS-2 PTC system are presented in Table 7. According to the results, there is a good agreement between the current study and the study of Mwesigye and Meyer [21], which can show the accuracy and reliability of the outputs of the present study.

5. Results and discussions

The simulation results of the PTC/PV system, OPTC/PV system with rotational absorber, and OPTC/PV system with both rotational absorber and copper metal foam are presented in this section. In this order, initially, the optimization of the PTC/PV system is performed using the Taguchi method. Afterward, the optimized system is simulated, and the effect of using a rotational absorber and copper foam on the thermal, electrical, and overall performance of the OPTC/PV system are assessed.

5.1. Optimization

As previously mentioned, for the optimization of the PTC/PV system, the Taguchi method is used. The considered parameters for the optimization are (A) the glass cover thickness, (B) the air gap thickness, (C) PV cell efficiency, and (D) mass fraction of the Cu nanoparticles. Also, it is considered that each parameter contains 4 different levels, which are presented in Table 8. Thus, due to the presence of 4 different parameters in the optimization, each of them contains 4 levels, there is needed to perform at least 13 simulations to determine the optimized system (Eq. (40)). However, the number of tests without using an optimization method is ($4^4 = 256$).

The number of simulations of the orthogonal array should be equal to

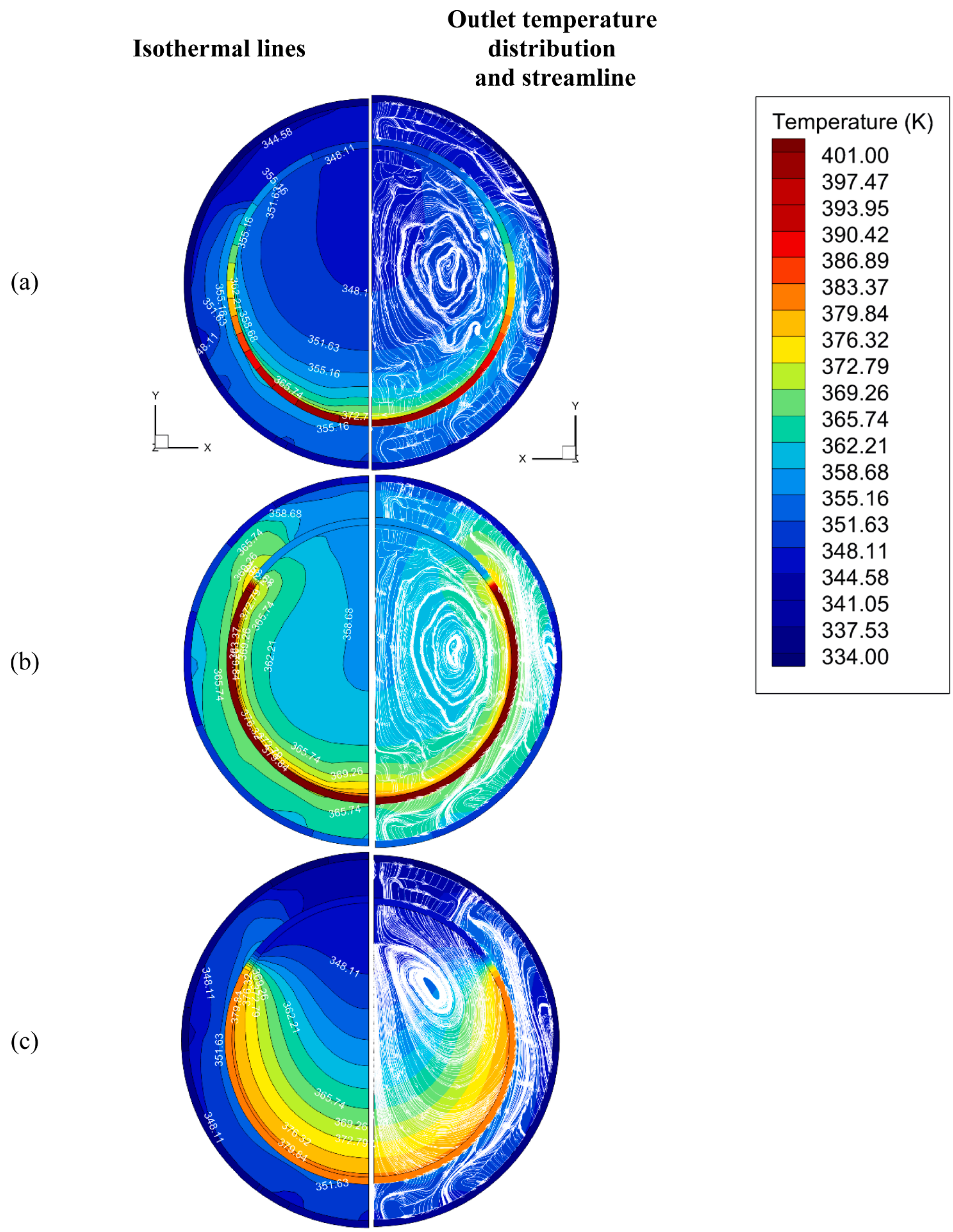

Fig. 9. The temperature distribution at the outlet of the receiver tube in the (a) OPTC/PV system, (b) OPTC/PV system with rotational absorber, and (c) OPTC/PV system with both rotational absorber and copper foam.

higher than the minimum number of tests (13 tests). In order to obtain the orthogonal array for system optimization, the Minitab 19 software is employed. The number of proposed tests for the optimization of the software is 25, which is higher than the minimum number of tests (25 > 13). Therefore, the proposed orthogonal array is suitable for optimization. In Table 9, the performed tests for the optimization of the PTC/PV system and their results are presented. Also, the amount of signal to noise (S/N) ratios for the studied parameters of the PTC/PV system is presented in Fig. 7.

In the Taguchi method, there are three ways to treat the amount of S/N ratio, including “the higher the better”, “the lower the better”, and “the nominal is better”. In this study, the objective parameter is overall efficiency; thus, the approach of “the higher the better” is chosen for optimizing the PTC/PV system. According to the selected approach, each parameter with the highest ratio of S/N is the best option for the system. As illustrated in Fig. 6, the highest amount of S/N ratio for the glass cover thickness, thickness of the air gap, PV cell efficiency, and nanoparticles mass fraction is 36.81 (Level 1), 36.82 (Level 2), 36.97 (Level 4), and 36.86 (Level 4), respectively. As a result, by simulation of the system and calculation of the overall efficiency (objectives parameter) of it, it is revealed that the PTC/PV system with the glass cover thickness of 2 mm, air gap thickness of 10 mm, PV cell efficiency of 21%, and nanoparticles mass fraction of 6% has the best possible performance. Besides, it is found that the variation of the PV cell efficiency and thickness of the glass cover has the highest and lowest influence on the functionality of the system, respectively.

5.2. The comparison between the cases

In this section, the effect of using a rotational absorber and installing copper foam inside the fluid channel on both the electrical and thermal performances of the OPTC/PV system are investigated. In this order, the output results of the OPTC/PV system, the OPTC/PV system with rotational absorber tube, and the OPTC/PV system with both copper foam and rotational absorber, are investigated and compared. It should be noted that these systems are simulated under the same working

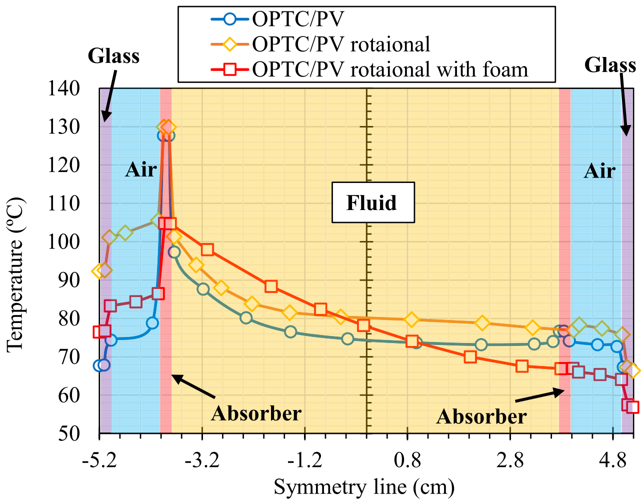

Fig. 10. The temperature distribution in the various layers of the system at the outlet of the receiver tube.

condition that the optimization process performed.

In Fig. 8, the operating fluid distribution of temperature at different cross-sections of the fluid channel of the systems are illustrated. These cross-sections are located at the distance of 0.25 m, 2.50 m, and 4.27 m from the inlet of the receiver tube. As indicated in Fig. 8(a), in the lower section of the outlet of the channel, the temperature of the fluid has its maximum value as a result of greater solar radiation intensity in this area (Fig. 2). However, by rotation of the absorber layer with the speed of $\omega = 0.5rad/s$ the distribution of the temperature near this layer gets more uniform (Fig. 8(b)). In the OPTC/PV system with a rotational absorber, the lower section of the tube that receives the greatest amount of solar radiation intensity changes by advance of time. Thus, the absorber can transfer a greater amount of energy to the fluid compared to the OPTC/PV system with a fixed absorber.

Additionally, in Fig. 8(c), it is obvious that the installation of copper foam in the fluid channel enhances the outlet temperature of the working fluid. Actually, adding copper foam to the fluid channel elevates the amount of heat conduction in the channel; thus, a greater amount of thermal energy transfers from the absorber layer to the operating fluid. However, the installation of foam to the OPTC/PV system with a rotational absorber declines the temperature of operating fluid in the upper section of the channel due to the resistance of the copper foam against the appearing secondary flow in the channel.

The distribution of temperature at the channel outlet for all systems are demonstrated in Fig. 9. As depicted in this figure, the maximum temperature belongs to the absorber layer where the solar radiation absorbs. According to the numerical simulations, the highest and lowest temperature at the receiver tube outlet belongs to the OPTC/PV system with rotational absorber and OPTC/PV system with both rotational absorber and cooper foam, respectively. In fact, in the OPTC/PV system with the rotational tube, a larger area of the tube is affected by the intense solar radiation concentration, while in the OPTC/PV system with a fixed absorber, a certain area is affected by the high solar radiation intensity, continuously. Additionally, in the OPTC/PV system with both

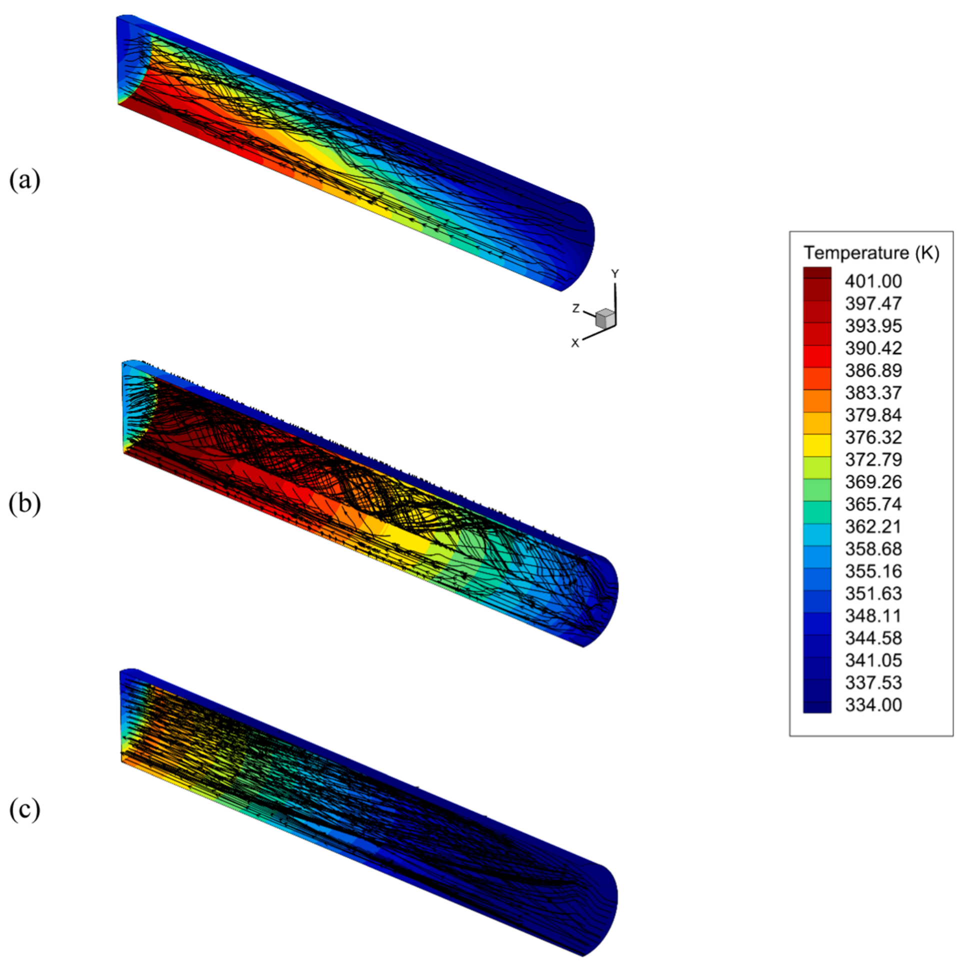

Fig. 11. The temperature distribution of the absorber layer in the (a) OPTC/PV system, (b) OPTC/PV system with rotational absorber, and (c) OPTC/PV system with both rotational absorber and copper foam.

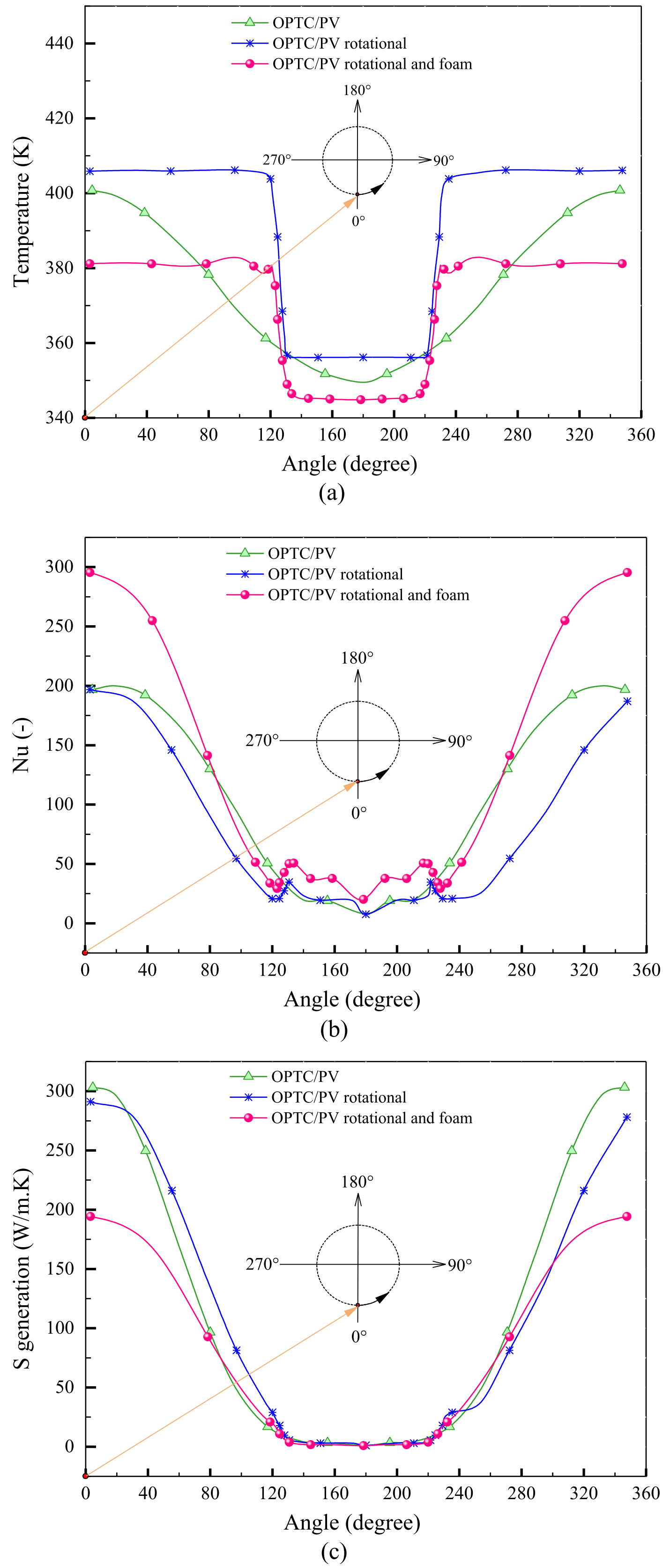

Fig. 12. (a) Temperature, (b) Nusselt number, and (c) entropy generation over the boundary of the fluid and absorber layer at the outlet of the receiver tube versus the receiver's angle in the different systems.

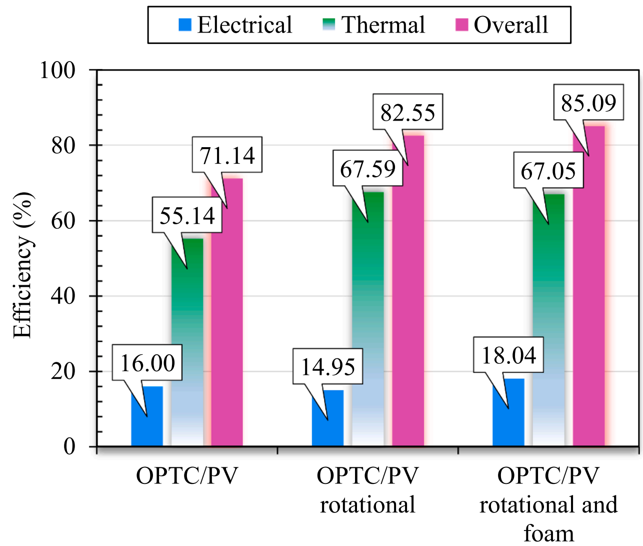

Fig. 13. The electrical, thermal, and overall electrical efficiency of the systems.

rotational absorber and cooper foam, due to the high thermal energy transfer from the absorber tube to the operating fluid, the temperature of the absorber layer does not increase considerably.

Besides, in Fig. 10, the temperature of the various layers of the systems on the symmetry line at the outlet of the receiver tube are depicted. As shown in this figure, the temperature of the operating fluid in the OPTC/PV system with both rotational tube and copper foam is more uniform in comparison to the other systems. As evident in this figure, the highest temperature in the system belongs to the absorber layer, where solar radiation absorbs. Also, the surface of the systems has the lowest temperature resulting from the heat transfer from the receiver to the surrounding ambient by both convection and conduction mechanisms.

In fact, in the OPTC/PV system with both rotational tube and copper foam, the temperature of the fluid declined from 104 °C in the lower section of the tube to 67 °C in the upper section of it. In contrast, the difference in temperature between the lower and upper section of the tube for the OPTC/PV system and OPTC/PV system with the rotational absorber is 51 °C and 52 °C, respectively. Besides, the temperature of the air media and glass layer has its maximum value in the OPTC/PV system, which shows the high loss of energy from the receiver tube to the ambient in this system.

Furthermore, the temperature distribution over the absorber layer of the systems is shown in Fig. 11. As mentioned earlier (section 2.5), increasing the PV cells temperature declines the output electrical power of the PV modules. Thus, a reduction in the temperature of the absorber layer causes more production of electrical energy by the system.

Additionally, the temperature, Nusselt number, and entropy generation on the boundary between the fluid and absorber layer at the receiver tube outlet versus the receiver's angle are demonstrated in Fig. 12(a), (b), and (c), respectively. As depicted in this figure, the temperature variation in the OPTC/PV system is much greater than in the other simulated systems. Actually, in the OPTC/PV system with a rotational absorber and OPTC/PV system with both a rotational absorber and copper foam, the amount of temperature in a vast area of the system is constant. This phenomenon is due to the rotational

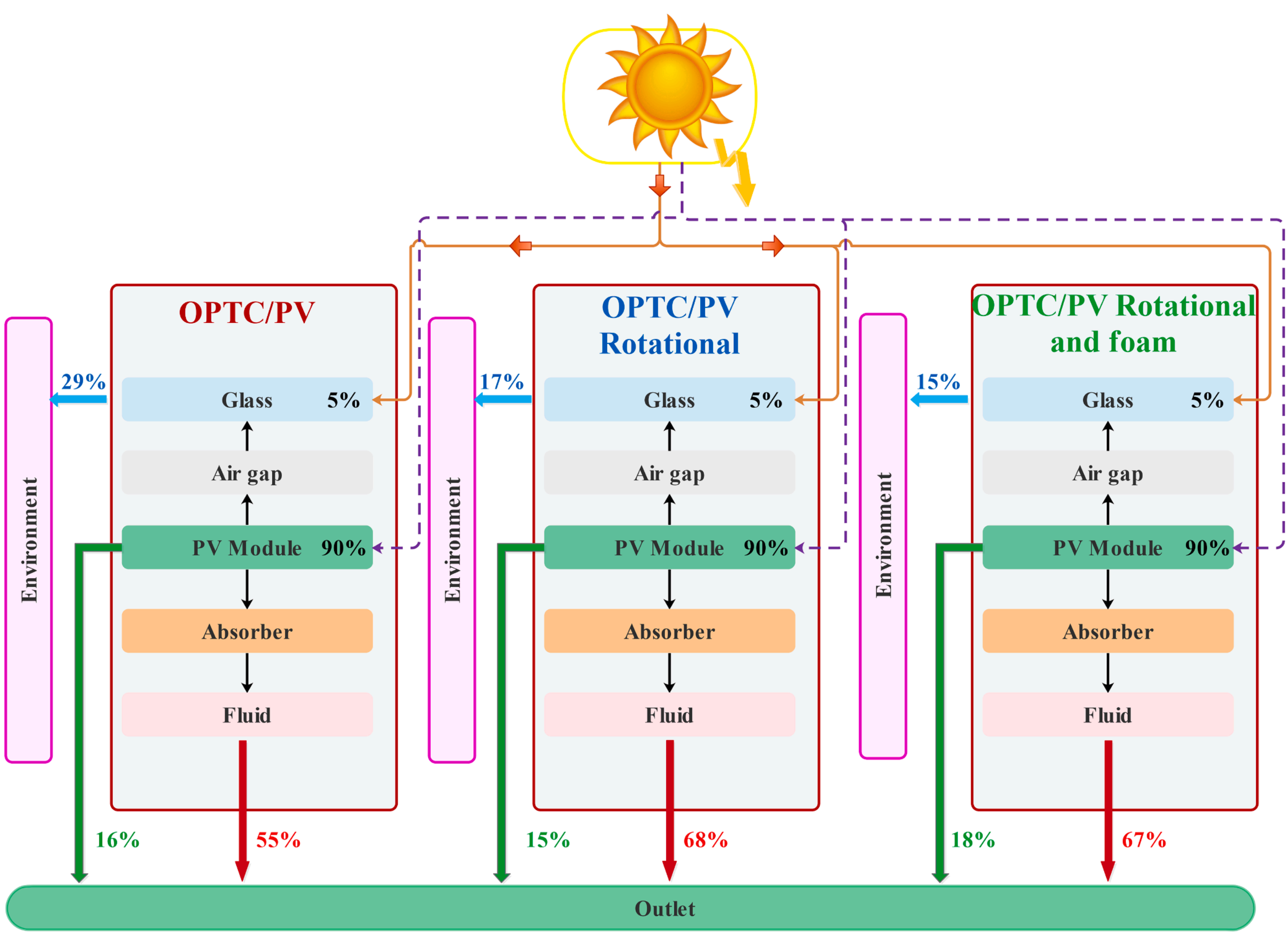

Fig. 14. The energy balance in the studied systems.

movement of the absorber and variations in the distribution of solar radiation over the absorber layer. Moreover, based on the distribution of the Nusselt number in different systems, by installing the copper foam and moving the absorber layer rotationally, the amount of Nusselt number in the system increases. However, the amount of Nusselt number in the OPTC/PV system with rotational absorber is lower than in the OPTC/PV system. Furthermore, based on the value of entropy generation in different systems, the rate of entropy generation in the OPTC/PV and OPTC/PV systems with rotational absorbers is almost the same. While installing copper foam in the fluid channel of the OPTC/PV system with a rotational absorber declines the entropy generation rate considerably.

Also, the electrical, thermal, and overall efficiencies of the systems are presented in Fig. 13. Based on the results obtained by simulations, the electrical efficiency of the OPTC/PV system, the OPTC/PV system with rotational absorber, and the OPTC/PV system with both rotational absorber and copper foam is 16.00%, 14.95%, and 18.04%, respectively. Additionally, the thermal efficiency of these systems is 55.14%, 67.59%, and 67.05%, respectively.

Although the temperature of the operating fluid in the OPTC/PV system with both rotational absorber and copper foam near the absorber layer is much higher than in other systems, the working temperature in the upper section of the tube is too low due to the absence of the secondary flow in the tube. Thus, the thermal efficiency of this system is lower than the OPTC/PV system with a rotational absorber overall. However, due to the PV module high electrical efficiency in the OPTC/PV system with both rotational absorber and copper foam, the overall efficiency of this system is higher than other systems. The overall efficiency of the OPTC/PV system, the OPTC/PV system with rotational absorber, and the OPTC/PV system with both rotational absorber and copper foam is 71.14%, 82.55%, and 85.09%, respectively. Moreover, the energy balance of all systems are depicted in Fig. 14.

As presented in Fig. 13, the amount of energy loss for the OPTC/PV system, OPTC/PV system with rotational absorber, and OPTC/PV system with both rotational absorber and copper foam is 29%, 17%, and 15%, respectively. According to the numerical simulations, the OPTC/PV system with rotational absorber and copper foam performs best among the studied cases.

6. Conclusion

Present study investigates the electrical, thermal, and overall performance of a PTC system integrated with a PV module (PTC/PV). In order to present an efficient hybrid system, the Taguchi method is implemented, and the influence of various parameters, including the air gap thickness, the thickness of the glass cover, the amount of nanofluid mass fraction, and the PV cell efficiency, on the performance of the system are evaluated. Also, for further enhancement of the performance of the PTC/PV system, the effect of rotating the receiver tube and installing metal foam inside the fluid channel on the outputs are investigated. Additionally, for better understanding of the performance of the systems, the temperature, Nusselt number, and entropy generation distribution at the cross sections of the systems are provided.

The most substantial findings of this paper can be presented as:

- The amount of variation in the S/N ratio of air gap thickness, glass thickness, nanoparticles mass fraction, and PV cell efficiency are 0.05, 0.05, 0.34, and 0.14, respectively. Therefore, the nanoparticles mass fraction is the most influential parameter on the functionality of the PTC/PV system.
- The PTC/PV system with the glass cover thickness of 2 mm, air gap thickness of 10 mm, PV cell efficiency of 21%, and nanoparticles mass fraction of 6% has the highest overall efficiency with a value of 71.14%.
- The overall efficiency of the OPTC/PV system, the OPTC/PV system with rotational absorber, and the OPTC/PV system with both rotational absorber and copper foam accounted to be 71.14%, 82.55%, and 85.09%, respectively.
- Although rotating the receiver tube enhances the system's overall performance, it reduces the thermal performance of the electrical efficiency of the system from 16.0% to 14.9%.
- Adding metal foam to the rotating receiver tube increases the system electrical efficiency from 14.9% to 18.0%, while it declines the system thermal performance by around 0.5%.

Currently, many solar power plants consist of the typical PTC systems; however, this type of solar power system provides only thermal energy. Also, the generated thermal power by the typical PTC system is not high enough.

The outputs of this investigation show that equipping the PTC system with a PV module, rotating receiver tube, and installing metal foam inside the fluid channel can remarkably improve the overall performance of this solar energy system. Therefore, this type of hybrid unit can be a proper alternative to the typical PTC systems in solar fields due to its higher performance. Also, this system can be installed in climates and locations even with low solar radiation intensity due to its capability to concentrate solar radiation on a receiver tube

Even though this study could take a significant step toward revealing the potential of using the PTC system, there are still some gaps that other researchers can fill. The recommended topics that can be studied in some other papers can be presented as follows:

- Analysis of the PTC/PV system from economic view point.
- Evaluating influence of using metal foam with different materials on the performance of the system from energy, exergy, and economic viewpoints.
- Scrutinizing the influence of nanoparticles material on the performance of the system and determining the optimum nanoparticle type.
- Experimental investigation of the effect of foam installation on the PTC system thermal performance.
- Evaluating the effect of rotating the absorber tube and filling the fluid channel with the metal foam with various porosities on the pressure drop of the receiver tube and energy consumption of the circulating pump.

CRediT authorship contribution statement

Gongxing Yan: Resources, Formal analysis, Investigation, Supervision. **Xia Zhou:** Writing – review & editing, Methodology, Formal analysis, Data curation. **Azher M. Abed:** Methodology, Writing – original draft, Investigation. **Theyab R Alsenani:** Methodology, Writing – original draft, Investigation. **Samia Elattar:** Writing – review & editing, Methodology, Formal analysis, Data curation. **Fan Peng:** Writing – review & editing, Methodology, Resources. **Mostafa A.H. Abdelmohimen:** Writing – review & editing, Formal analysis, Resources.

Declaration of Competing Interest

The authors declare that they have no known competing financial interests or personal relationships that could have appeared to influence the work reported in this paper.

Data availability

No data was used for the research described in the article.

Acknowledgments

- The authors extend their appreciation to the Deanship of Scientific Research at King Khalid University for funding this work through Large Groups (RGP.2/94/43)
- This work was supported by Sichuan Province Luzhou city of Stars science and technology planning project(2022-GYF-16), and the scientific research and innovation team construction project of Luzhou vocational and Technical College (2021YJTD07).
- The author (Azher M.Abed) extends his appreciation to the Deanship of Al-Mustaqbal University College for funding this work through the grant number MUC-E-0122.
- Princess Nourah bint Abdulrahman University Researchers Supporting Project number (PNURSP2023R163), Princess Nourah bint Abdulrahman University, Riyadh, Saudi Arabia.
- This research was supported by the Deanship of Scientific Research at Prince Sattam Bin Abdulaziz University.

References

[1] M. Chafie, M.F.B. Aissa, S. Bouadila, M. Balghouthi, A. Farhat, A. Guizani, Experimental investigation of parabolic trough collector system under Tunisian climate: design, manufacturing and performance assessment, Appl. Therm. Eng. 101 (2016) 273–283, https://doi.org/10.1016/j.applthermaleng.2016.02.073.

[2] M.T. Jamal-Abad, S. Saedodin, M. Aminy, Experimental investigation on a solar parabolic trough collector for absorber tube filled with porous media, Renew. Energy 107 (2017) 156–163.

[3] M. Valizade, M. Heyhat, M. Maerefat, Experimental study of the thermal behavior of direct absorption parabolic trough collector by applying copper metal foam as volumetric solar absorption, Renew. Energy 145 (2020) 261–269, https://doi.org/10.1016/j.renene.2019.05.112.

[4] Y. Qiu, M.-J. Li, Y.-L. He, W.-Q. Tao, Thermal performance analysis of a parabolic trough solar collector using supercritical CO2 as heat transfer fluid under non-uniform solar flux, Appl. Therm. Eng. 115 (2017) 1255–1265, https://doi.org/10.1016/j.applthermaleng.2016.09.044.

[5] E. Bellos, C. Tzivanidis, V. Belessiotis, Daily performance of parabolic trough solar collectors, Sol. Energy 158 (2017) 663–678, https://doi.org/10.1016/j.solener.2017.10.038.

[6] E. Bellos, C. Tzivanidis, A detailed exergetic analysis of parabolic trough collectors, Energ. Conver. Manage. 149 (2017) 275–292, https://doi.org/10.1016/j.enconman.2017.07.035.

[7] A. Raheem, W. Siddique, Z.H. Farooqui, T. Salameh, I.-U. Haq, K. Waheed, K. Qureshi, Performance evaluation of adding helical-screw tape inserts in parabolic solar trough collectors as a source of cleaner energy production, J. Clean. Prod. (2021), 126628, https://doi.org/10.1016/j.jclepro.2021.126628.

[8] S. Guillén-Lambea, M. Carvalho, A critical review of the greenhouse gas emissions associated with parabolic trough concentrating solar power plants, J. Clean. Prod. (2021), 125774, https://doi.org/10.1016/j.jclepro.2020.125774.

[9] A. Salari, A. Taheri, A. Farzanehnia, M. Passandideh-fard, M. Sardarabadi, An updated review of the performance of nanofluid-based photovoltaic thermal systems from energy, exergy, economic, and environmental (4E) approaches, J. Clean. Prod. 282 (2021), 124318, https://doi.org/10.1016/j.jclepro.2020.124318.

[10] A. Allouhi, M.B. Amine, R. Saidur, T. Kousksou, A. Jamil, Energy and exergy analyses of a parabolic trough collector operated with nanofluids for medium and high temperature applications, Energ. Conver. Manage. 155 (2018) 201–217, https://doi.org/10.1016/j.enconman.2017.10.059.

[11] M. Bezaatpour, H. Rostamzadeh, J. Bezaatpour, Hybridization of rotary absorber tube and magnetic field inducer with nanofluid for performance enhancement of parabolic trough solar collector, J. Clean. Prod. 283 (2021), 124565, https://doi.org/10.1016/j.jclepro.2020.124565.

[12] M. Sardarabadi, M. Passandideh-Fard, S.Z. Heris, Experimental investigation of the effects of silica/water nanofluid on PV/T (photovoltaic thermal units), Energy 66 (2014) 264–272, https://doi.org/10.1016/j.energy.2014.01.102.

[13] M. Sarafraz, M.R. Safaei, A.S. Leon, I. Tlili, T.A. Alkanhal, Z. Tian, M. Goodarzi, M. Arjomandi, Experimental Investigation on thermal performance of a PV/T-PCM (photovoltaic/thermal) system cooling with a PCM and nanofluid, Energies 12 (2019) 2572, https://doi.org/10.3390/en12132572.

[14] A.H.A. Al-Waeli, M.T. Chaichan, K. Sopian, H.A. Kazem, H.B. Mahood, A. A. Khadom, Modeling and experimental validation of a PVT system using nanofluid coolant and nano-PCM, Sol. Energy 177 (2019) 178–191, https://doi.org/10.1016/j.solener.2018.11.016.

[15] A. Salari, A. Hakkaki-Fard, A numerical study of dust deposition effects on photovoltaic modules and photovoltaic-thermal systems, Renew. Energy 135 (2019) 437–449, https://doi.org/10.1016/j.renene.2018.12.018.

[16] A. Salari, A. Parcheforosh, A. Hakkaki-Fard, A. Amadeh, A numerical study on a photovoltaic thermal system integrated with a thermoelectric generator module, Renew. Energy (2020), https://doi.org/10.1016/j.renene.2020.02.018.

[17] S. Soltani, A. Kasaeian, T. Sokhansefat, M.B. Shafii, Performance investigation of a hybrid photovoltaic/thermoelectric system integrated with parabolic trough collector, Energ. Conver. Manage. 159 (2018) 371–380, https://doi.org/10.1016/j.enconman.2017.12.091.

[18] M. Valizadeh, F. Sarhaddi, M.M. Adeli, Exergy performance assessment of a linear parabolic trough photovoltaic thermal collector, Renew. Energy 138 (2019) 1028–1041, https://doi.org/10.1016/j.renene.2019.02.039.

[19] H. Pierrick, M. Christophe, G. Leon, D. Patrick, Dynamic numerical model of a high efficiency PV–T collector integrated into a domestic hot water system, Sol. Energy 111 (2015) 68–81, https://doi.org/10.1016/j.solener.2014.10.031.

[20] J.J. Michael, I. Selvarasan, R. Goic, Fabrication, experimental study and testing of a novel photovoltaic module for photovoltaic thermal applications, Renew. Energy 90 (2016) 95–104, https://doi.org/10.1016/j.renene.2015.12.064.

[21] A. Mwesigye, J.P. Meyer, Optimal thermal and thermodynamic performance of a solar parabolic trough receiver with different nanofluids and at different concentration ratios, Appl. Energy 193 (2017) 393–413, https://doi.org/10.1016/j.apenergy.2017.02.064.

[22] M. Hosseinzadeh, A. Salari, M. Sardarabadi, M. Passandideh-Fard, Optimization and parametric analysis of a nanofluid based photovoltaic thermal system: 3D numerical model with experimental validation, Energ. Conver. Manage. 160 (2018) 93–108, https://doi.org/10.1016/j.enconman.2018.01.006.

[23] A. Salari, A. Taheri, A. Farzanehnia, M. Passandideh-fard, M. Sardarabadi, An updated review of the performance of nanofluid-based photovoltaic thermal systems from energy, exergy, economic, and environmental (4E) approaches, J. Clean. Prod. 124318 (2020), https://doi.org/10.1016/j.jclepro.2020.124318.

[24] B.C. Pak, Y.I. Cho, Hydrodynamic and heat transfer study of dispersed fluids with submicron metallic oxide particles, Exp. Heat Transfer Int. J. 11 (1998) 151–170, https://doi.org/10.1080/08916159808946559.

[25] Y. Xuan, Q. Li, W. Hu, Aggregation structure and thermal conductivity of nanofluids, AIChE J 49 (2003) 1038–1043, https://doi.org/10.1002/aic.690490420.

[26] M. Corcione, Empirical correlating equations for predicting the effective thermal conductivity and dynamic viscosity of nanofluids, Energ. Conver. Manage. 52 (2011) 789–793, https://doi.org/10.1016/j.enconman.2010.06.072.

[27] D.T. Lobera, S. Valkealahti, Dynamic thermal model of solar PV systems under varying climatic conditions, Sol. Energy 93 (2013) 183–194, https://doi.org/10.1016/j.solener.2013.03.028.

[28] J.A. Duffie, W.A. Beckman, N. Blair, Solar Engineering of Thermal Processes, Photovoltaics and Wind, John Wiley & Sons (2020), https://doi.org/10.1002/9781119540328.

[29] A. Fluent, Ansys fluent theory guide, Ansys Inc., USA, 15317 (2011) 724–746.

[30] T.-H. Shih, W.W. Liou, A. Shabbir, Z. Yang, J. Zhu, A new k-ϵ eddy viscosity model for high reynolds number turbulent flows, Comput. Fluids 24 (1995) 227–238, https://doi.org/10.1016/0045-7930(94)00032-T.

[31] A. Kazemian, M. Khatibi, T. Ma, J. Peng, Y. Hongxing, A thermal performance-enhancing strategy of photovoltaic thermal systems by applying surface area partially covered by solar cells, Appl. Energy 329 (2023), 120209, https://doi.org/10.1016/j.apenergy.2022.120209.

[32] S. Mullick, S. Nanda, An improved technique for computing the heat loss factor of a tubular absorber, Sol. Energy 42 (1989) 1–7, https://doi.org/10.1016/0038-092X(89)90124-2.

[33] W.C. Swinbank, Long-wave radiation from clear skies, Q. J. R. Meteorolog. Soc. 89 (1963) 339–348, https://doi.org/10.1002/qj.49708938105.

[34] T.L. Bergman, A.S. Lavine, F.P. Incropera, D.P. DeWitt, Introduction to Heat Transfer, John Wiley & Sons, 2011.

[35] M. Libra, T. Petrík, V. Poulek, I.I. Tyukhov, P. Kouřím, Changes in the efficiency of photovoltaic energy conversion in temperature range with extreme limits, IEEE J. Photovoltaics 11 (2021) 1479–1484, https://doi.org/10.1109/JPHOTOV.2021.3108484.

[36] A. Kazemian, A. Salari, T. Ma, A year-round study of a photovoltaic thermal system integrated with phase change material in Shanghai using transient model, Energ. Conver. Manage. 210 (2020), 112657, https://doi.org/10.1016/j.enconman.2020.112657.

[37] D. Evans, Simplified method for predicting photovoltaic array output, Sol. Energy 27 (1981) 555–560, https://doi.org/10.1016/0038-092X(81)90051-7.

[38] A. Bejan, Entropy generation minimization: the method of thermodynamic optimization of finite-size systems and finite-time processes, CRC Press (2013), https://doi.org/10.1201/9781482239171.

[39] C.-F.-J. Kuo, J.-M. Liu, M.L. Umar, W.-L. Lan, C.-Y. Huang, S.-S. Syu, The photovoltaic-thermal system parameter optimization design and practical verification, Energ. Conver. Manage. 180 (2019) 358–371, https://doi.org/10.1016/j.enconman.2018.10.080.

[40] H. Bas, V. Ozceyhan, Optimization of parameters for heat transfer and pressure drop in a tube with twisted tape inserts by using Taguchi method, Arab. J. Sci. Eng. 39 (2014) 1177–1186, https://doi.org/10.1007/s13369-013-0648-4.

[41] V. Verma, K. Murugesan, Optimization of solar assisted ground source heat pump system for space heating application by Taguchi method and utility concept, Energ. Buildings 82 (2014) 296–309, https://doi.org/10.1016/j.enbuild.2014.07.029.

[42] C.-F.-J. Kuo, T.-L. Su, P.-R. Jhang, C.-Y. Huang, C.-H. Chiu, Using the Taguchi method and grey relational analysis to optimize the flat-plate collector process with multiple quality characteristics in solar energy collector manufacturing, Energy 36 (2011) 3554–3562, https://doi.org/10.1016/j.energy.2011.03.065.

[43] V.E. Dudley, G.J. Kolb, A.R. Mahoney, T.R. Mancini, C.W. Matthews, M. Sloan, D. Kearney, Test results: SEGS LS-2 solar collector, in, Sandia National Lab.(SNL-NM), Albuquerque, NM (United States), 1994.